Available online at www.sciencedirect.com
ScienceDirect
Journal of Sound and Vibration 307 (2007) 113–138
JOURNAL OF SOUND AND VIBRATION
www.elsevier.com/locate/jsvi

Source effects on attenuation in lined ducts. Part I: A statistically based computational approach

Gabriel Zlavog, Walter Eversman*

Mechanical and Aerospace Engineering, University of Missouri-Rolla, Rolla, MO 65401, USA

Accepted 26 June 2007
The peer review of this article was organised by the Guest Editor

Abstract

The influence of the source on acoustic attenuation in uniform and non-uniform ducts with mean flow is investigated. It is found that realizable attenuation is sensitive to details of the source that in applications such as broadband noise may be unavailable. In this investigation a statistical source model is proposed. A finite element simulation for propagation in non-uniform ducts with compressible mean flow with a random source description is developed. Probability density functions for transmitted acoustic power and attenuation are determined based on as many as 100,000 trials with random distributions of input modal power and phase. For cases with a moderate to large number of input modes, transmitted power and attenuation appear to follow simple statistical distributions. A comparison is made with limited experimental data, and in all cases considered measured attenuation is within or close to the predicted distribution.

1. Introduction

Emergence of the turbofan and later the high bypass ratio turbofan engine as the main alternative for civil aviation had the effect of reducing jet noise, while increasing fan-compressor noise. Reduction in fan noise has been achieved to some extent by the use of acoustic treatment; however, fan noise continues to be a problem to be dealt with at both takeoff and approach.

Design optimization of acoustic treatment has been a problem of interest since the early work of Cremer [1]. His approach was limited to ducts with no flow and was based on impedance maps plotting contours of equal attenuation. This approach still has applicability in current problems including the effect of mean flow. With increase in emphasis on jet and turbofan noise control in the 1970s, the method of Rice [2] based on duct modal attenuation, its correlation with mode cut-off ratio, and modal acoustic power became the accepted design standard. Recent methods for modeling of propagation in realistic nacelle geometry include finite element models [3], ray theory [4], and a parabolized wave equation approximation [5].

Current studies have resulted in the observation that predicted optimum impedance is not consistent among the various models. Furthermore, comparison of predicted attenuations with experimental data has shown

*Corresponding author. Tel.: +1 573 341 4670; fax: +1 573 341 4607.
E-mail address: eversman@umr.edu (W. Eversman).

0022-460X/$ - see front matter © 2007 Elsevier Ltd. All rights reserved.
doi:10.1016/j.jsv.2007.06.031

little systematic correlation. While all propagation models are based on a common physical model (with various approximations), they diverge when source representation is considered. Sensitivity of attenuation realized by acoustic treatment to source description is the focus of this investigation.

Lack of data for modal distribution has led researchers to make simplifying assumptions about the source. In an early study, Rice [6] assumed a plane traveling wave, accounting for a pressure distribution of equal magnitude and phase in all radial modes. The acoustic field inside the lined section is obtained and matched to the assumed pressure distribution at the ends. Snow [7] investigated differences in attenuation for three different source models: a planar wave, a modal distribution with pressure proportional to the blade local velocity and finally, a distribution with phase varying linearly and constant amplitude across the duct. Studying the effect of shear layer on attenuation, Mariano [8] tested a diffuse sound field, considering the modal amplitudes to be the same at the entrance of the test section. He acknowledged that the phases should be randomly distributed, but no provision was made to take this fact into account.

Rice [9] obtained a simplified formula for the mean square far-field radiated pressure. He proposed a biasing function to alter the acoustic radial power distribution in the inverse powers of the cut-off ratio. Rice showed that inlet broadband noise experimental data for radiation patterns seemed to fit the equal acoustic power per mode theory. Tonal noise radiation patterns investigated data that fitted a shift of power toward modes with low cut-off ratio. However, the far-field acoustic power flux considers the sum of all modal pressures with their individual phase such that intermodal pressure cancellations due to phase can occur, making the method presented in the study valid only in the particular case when the modes are phase correlated.

Modal structure of sound generated by blade-vane interactions is essential in prediction of in-duct propagation and radiation directivity patterns of tonal noise. In this case, a relatively limited number of modes are dominant and theoretical predictions or experiment may ultimately yield a reliable model of the source. In the case of broadband noise, produced by sources random in time or location, the modal source description probably cannot be estimated. In either case, at the present time the details of the source must be considered incomplete.

The present study, which is a continuation of a previous investigation [10], is an extended analysis of both source magnitude and phase variations and their influence on achieved attenuation in lined ducts. A concurrent investigation to be published in a companion paper will examine in more detail the statistical distribution of realized attenuation.

In this paper, three methods are used to assess the performance of acoustic treatment. The first is based on the Cremer method and deals with infinite duct eigenvalues and eigenmodes. Optimization is achieved by maximizing the attenuation in the least attenuated mode. The method is simple because it considers an infinitely long uniform duct, which is an approximation of the actual duct geometry and mean flow conditions. The duct eigenvalue calculation involves only modal attenuations and considers neither modal amplitudes nor phases.

The other two lining assessment methods described here require specification of modal input and results obtained depend strongly on this information. When source input is required, accurate information about the modal content of the source is needed. In its absence, in the present study we propose statistical random modal power and phase distributions that can be combined with certain simplifying assumptions about the nature of the source. In this sense the following options are tested:

- equal incident modal power and phase;
- equal incident modal power and random phase;
- random incident modal power and equal phase;
- biased incident modal power distribution among modes (defined on the basis of the cut-off ratio) and equal phase;
- biased incident modal power distribution among modes and random phase;
- random incident modal power and random phase.

These options have been provided in codes referred to as the segmented duct code and the propagation code. In these approaches, the duct is considered to have a hard wall source section, a lined section and a hard wall exit section. Acoustic power transmission loss is the measure of lining performance.

The segmented duct code models the duct as uniform in cross section. The mean flow does not vary in the axial direction, but it can vary in the radial direction to model the velocity profile of a sheared boundary layer. Acoustic modes in the lined and unlined sections of the duct, together with the associated axial wavenumbers, are obtained using a finite element model that takes into account the impedance in the lined section. Sections of the duct are coupled by imposing continuity of acoustic mass flux and acoustic momentum. A reflection free termination is assumed at the rigid exit section, so that only outgoing modes are present. Incident modes are specified through their complex modal amplitudes at the source plane. Reflected modal amplitudes are calculated at the source section, as well as transmitted modal amplitudes at the exit side. Modal amplitudes in the lined section are also calculated. Acoustic power is determined based on the incident, reflected and transmitted modal amplitudes.

In the propagation code, the geometry of any non-uniform duct can be accurately represented. Two straight rigid wall sections adjoin the non-uniform section, a portion of which is acoustically lined. The mean flow, if present, is compressible potential flow, consistent with the duct geometry. The acoustic field in the duct is described by a finite element discretization, the geometry being assumed axi-symmetric. The eigenproblem developed from the acoustic field equations is the basis for calculating the acoustic modes at the source plane and at the termination plane. The incident modal amplitudes, with their phases, are specified and they represent the source. Transmitted and reflected mode amplitudes are calculated and used to complete the source and termination description.

2. Mathematical models for acoustic propagation

Analysis methods used in this study are based on a common starting point. It is assumed that acoustic propagation is modeled by small perturbations on a steady, isentropic, irrotational compressible mean flow. The duct is axi-symmetric and the coordinate system is cylindrical, with x the axis of symmetry, θ the circumferential coordinate, and r the cylindrical radius. The mean flow satisfies the continuity and momentum equations, and the isentropic equation of state in the form

$$\nabla \cdot \left(\rho_r \nabla \phi_r\right) = 0, \tag{1}$$

$$\rho_r = \left[1 + \frac{\gamma - 1}{2}(M_\infty^2 - \nabla\phi_r \cdot \nabla\phi_r)\right]^{\frac{1}{\gamma-1}}, \tag{2}$$

$$c_r^2 = \rho_r^{\gamma-1} = 1 + \frac{\gamma - 1}{2}(M_\infty^2 - \nabla\phi_r \cdot \nabla\phi_r). \tag{3}$$

The steady flow field equations are in non-dimensional form based on conditions at the acoustic source plane where the Mach number is M_∞, density is ρ_∞, and speed of sound is c_∞. Local (non-dimensional or reference) density and speed of sound are $\rho_r = \rho/\rho_\infty$, $c_r = c/c_\infty$, and local non-dimensional Mach number is $M_r = V/c_\infty = \left|\nabla\phi_r\right|$. V is the local flow speed and ϕ_r is the local velocity potential, non-dimensional with respect to Rc_∞. R is a reference length, in the present case the duct radius at the source plane. Spatial variables are non-dimensional with respect to R. For uniform flow cases, density, speed of sound and Mach number are constant and equal to ρ_∞, c_∞, M_∞. For non-uniform ducts Eqs. (1)–(3) are solved by the method of weighted residuals in a finite element formulation [11,12]. Acoustic perturbations are represented in terms of the linearized continuity equation in terms of acoustic potential $\vec{v} = \nabla\phi$

$$\frac{\partial\rho}{\partial t} + \nabla \cdot (\rho_r \nabla\phi + \rho \nabla\phi_r) = 0. \tag{4}$$

Pressure and density follow from the acoustic momentum equation and the acoustic equation of state:

$$p = -\rho_r\left(\frac{\partial\phi}{\partial t} + \nabla\phi_r \cdot \nabla\phi\right), \tag{5}$$

$$\rho = -\frac{\rho_r}{c_r^2}\left(\frac{\partial\phi}{\partial t} + \nabla\phi_r \cdot \nabla\phi\right). \tag{6}$$

Acoustic perturbations are non-dimensional on the same basis as steady flow field variables, with the addition that acoustic pressure is non-dimensional with respect to $\rho_\infty c_\infty^2$.

The boundary conditions at an impedance wall relating the normal component of acoustic particle velocity to displacement of the boundary in non-dimensional form are

$$\vec{v}\cdot\vec{n} = \nabla\phi\cdot\vec{n} = \frac{\partial\zeta}{\partial t} + \vec{M}_r\cdot\mathrm{grad}\zeta - \zeta\vec{n}\cdot(\vec{n}\cdot\mathrm{grad})\vec{M}_r. \tag{7}$$

Non-dimensional displacement at the boundary is denoted by ζ, and is in the direction $\vec{n}$ normal (outward) to the undeformed surface [13]. At the wall there is an impedance relationship connecting acoustic pressure at the wall to the velocity of the boundary. In harmonic motion this is in non-dimensional form

$$p = Z\frac{\partial\zeta}{\partial t} = \mathrm{i}\eta_r Z\zeta. \tag{8}$$

Consistent with harmonic motion, differentiation with respect to time, $\partial\zeta/\partial t$ is replaced by $\mathrm{i}\eta_r\zeta$, with $\eta_r = \omega R/c_\infty$ defined as the non-dimensional frequency. ω is the dimensional frequency in rad/sec. In Eq. (8), Z is the impedance, made non-dimensional after dividing by $\rho_\infty c_\infty$.

For a uniform duct in the case of harmonic dependence, this general formulation leads to the convected wave equation [14]

$$\left(\mathrm{i}\eta_r + M_r\frac{\partial}{\partial x}\right)^2 p - \nabla^2 p = 0, \tag{9}$$

and for a circular duct, boundary conditions

$$\frac{\partial p}{\partial r} = -\frac{\mathrm{i}\eta_r}{Z}\left(1 - \mathrm{i}\frac{M_r}{\eta_r}\frac{\partial}{\partial x}\right)^2 p, \quad r = 1, \quad p \text{ is finite}, \quad r = 0. \tag{10}$$

At the inner wall of an annular duct, a similar boundary condition is applicable. Duct modes are found from an eigen-problem defined by Eqs. (9) and (10) when a solution is assumed in the form

$$p = P(r)\mathrm{e}^{-\mathrm{i}(m\theta + k_x x)}. \tag{11}$$

The eigen-problem for the circular duct [14] is then to find for a specified circumferential mode, m, and a specified frequency η_r, non-trivial solutions to

$$\begin{aligned} &\frac{\mathrm{d}^2 P}{\mathrm{d}r^2} + \frac{1}{r}\frac{\mathrm{d}P}{\mathrm{d}r} + \left(\kappa^2 - \frac{m^2}{r^2}\right)P = 0,\\ &\frac{\mathrm{d}P}{\mathrm{d}r} = -\frac{\mathrm{i}\eta_r}{Z}\left(1 - M_r\frac{k_x}{\eta_r}\right)^2 P, \quad r = 1,\\ &P \text{ is finite}, \quad r = 0, \end{aligned} \tag{12}$$

where the axial wavenumber is defined by

$$\frac{k_x}{\eta_r} = \frac{1}{1 - M_r^2}\left[-M_r \pm \sqrt{1 - (1 - M_r^2)\left(\frac{\kappa}{\eta_r}\right)^2}\right]. \tag{13}$$

k_x/η_r is in general complex with the real part corresponding to phase velocity and the imaginary part corresponding to attenuation. A similar eigen-problem is obtained for the case of an annular duct with the additional inner wall boundary condition.

Axial wavenumbers are grouped according to direction of propagation. Those yielding decay in the positive x direction are classified as right running waves and those yielding decay in the negative x direction are classified as left running waves. Within the two classifications axial wavenumbers are ordered according to the ascending magnitude of the attenuation. The least attenuated radial mode for a specified angular mode

(wavenumber) is mode $n = 1$. Eqs. (12) and (13) form the basis for what is referred to here as the Cremer optimization method. In the original work of Cremer [1] the mean flow was not considered. His approach would be equivalent to plotting contours of equal attenuation in the impedance plane with axes taken as resistance and reactance of the wall impedance Z. The Cremer approach used here includes mean flow and couples the eigen-problem to an optimization scheme which seeks the impedance which produces the maximum attenuation in the least attenuated mode propagating away from the source. After finding the optimum, the map of attenuation contours in the impedance plane is produced, centered on the optimum.

The eigen-problem of Eq. (12) is based on the Bessel equation, and in principle a semi-analytic approach to solution is possible. However, it proves to be far more efficient to use a weighted residual scheme based on the finite element method to generate a discrete algebraic eigenvalue problem from Eqs. (12) and (13).

The segmented duct code is also based on the eigen-problem of Eqs. (12) and (13). In this case, the duct is divided into three segments, beginning with a hard wall (infinite impedance) source section, an acoustically treated section and a hard wall termination section with non-reflecting exit. This is shown in Fig. 1. The flow in the figure is from left to right (positive Mach number). The acoustic field at the source is a combination of incident (positive) and reflected (negative) complex pressure amplitudes a_1^+ and a_1^-. At the left interface between the hard wall and the acoustically treated section b_1^+ represents the incident amplitudes while b_1^- the reflected ones, a_2^+ signifies the transmitted amplitudes in the lined section and a_2^- the reflected ones. At the right interface b_2^+ and b_2^- are the incident and reflected soft wall amplitudes, a_3^+ and a_3^- are the transmitted and reflected amplitudes in the terminating hard wall section. b_3^+ and b_3^- are transmitted and reflected amplitudes at the end of the terminating hard wall section. It is assumed that the end of the duct is reflection free such that $b_3^- = 0$.

In each section, the eigen-problem is solved to determine a finite set of axial wavenumbers and eigenfunctions. The eigenfunctions are defined at discrete points, the nodes of the finite element mesh. Continuous versions of the eigenfunctions are obtained by conventional finite element interpolation. In each section the acoustic field is represented by an eigenfunction expansion based on a set of right and left running modes, the number of which is chosen to span all propagating modes plus a few cut-off modes. Amplitudes of the modes are the coefficients shown in Fig. 1. Incident mode amplitudes a_1^+ are specified and reflected modes b_3^- vanish to enforce the condition of no reflection. At the interfaces between the hard and soft wall sections continuity of acoustic mass and conservation of acoustic momentum (axial component) are enforced via a weighted residuals formulation.

The resulting set of algebraic equations produces the unknown modal amplitudes, which are organized in the form of transmission and reflection matrices. For example, an overall transmission matrix would be

$$\{a_3^+\} = [T]\{a_1^+\}, \tag{14}$$

and an overall reflection matrix would be

$$\{a_1^-\} = [R]\{a_1^+\}. \tag{15}$$

Other scattering matrices can be defined to obtain, for example, $\{a_2^+\}$ and $\{a_2^-\}$ defining the scattered field in the lined section.

In the segmented duct code, the performance metric is based on acoustic power. At the source plane and exit plane, acoustic power is accurately calculated with the use of hard wall eigenfunctions and axial wavenumbers

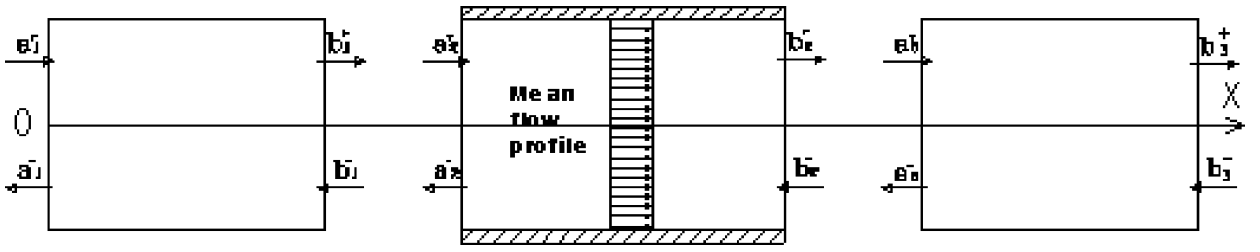

Fig. 1. Segmented duct showing modal amplitude coefficients in each section and a mean flow profile.

[11,12] when the flow is uniform. Acoustic power at the source $x = 0$ can be written, using the definition of Morfey [15], based on power matrices and the modal amplitude coefficients

$$\Pi_0 = \{a_1^{+^*}\}^{\mathrm{T}}[P_0^{++}]\{a_1^{+}\} + \{a_1^{+^*}\}^{\mathrm{T}}[P_0^{+-}]\{a_1^{-}\} + \{a_1^{-^*}\}^{\mathrm{T}}[P_0^{-+}]\{a_1^{+}\} + \{a_1^{-^*}\}^{\mathrm{T}}[P_0^{--}]\{a_1^{-}\}, \tag{16}$$

where a complex conjugate is denoted by superscript * and a transpose by superscript T. If cut-off modes are not included, the power at the source plane is due to incident and reflected propagating modes and

$$\Pi_0 = \{a_1^{+^*}\}^{\mathrm{T}}[P_0^{++}]\{a_1^{+}\} + \{a_1^{-^*}\}^{\mathrm{T}}[P_0^{--}]\{a_1^{-}\}. \tag{17}$$

At the duct exit $x = L$, the power can be expressed in terms of the transmitted modal amplitudes, because there are no reflected modes

$$\Pi_L = \{b_2^{+^*}\}^{\mathrm{T}}[P_L^{++}]\{b_2^{+}\}. \tag{18}$$

The power matrices at $x = 0$, $[P_0^{++}]$, $[P_0^{--}]$, are diagonal and so is the power matrix at $x = L$, $[P_L^{++}]$.

If a sheared flow profile is assumed, a measure of acoustic power based on the integration of the mean squared pressure on the cross section is used. There is no simple conservation law in this case, but in this seldom used option, useful results seem to be obtained. If the transmitted modes are rewritten, relating them to the source modal amplitudes with the help of the transmission matrix from Eq. (14), then

$$\Pi_L = \{a_1^{+^*}\}^{\mathrm{T}}[T^*]^{\mathrm{T}}[P_L^{++}][T]\{a_1^{+}\}. \tag{19}$$

The power transmission coefficient, as a measure of the lining performance is defined by

$$\mathrm{TC} = \frac{\Pi_L}{\Pi_0}, \tag{20}$$

and the acoustic power attenuation, expressed in decibels is

$$\mathrm{Atten} = -10\log_{10}\mathrm{TC}. \tag{21}$$

For the propagation code, the duct and mean flow field are non-uniform. A representation of the acoustic field is no longer based on an eigenfunction expansion throughout the duct. The numerical model for duct propagation is based on a finite element discretization of the steady flow field Eqs. (1)–(3) and the acoustic field Eqs. (4)–(7) on an axi-symmetric domain. The steady compressible flow field is obtained from a weighted residuals/Galerkin FEM formulation in terms of velocity potential of Eq. (1), the continuity equation, linearized at each step of an iterative process with density allowed to be spatially dependent. Eqs. (2) and (3) are subsidiary relations used to update density and speed of sound at each step. Mass flow rate is specified on the source plane and the exit plane is assumed an equi-potential surface. The mean flow field is described in terms of the mean flow velocity potential, which is required as input data for the acoustic FEM model. The mean flow mesh is the same as the acoustic mesh to simplify data transfer.

The finite element model for acoustic propagation is also a weighted residuals/Galerkin formulation based on Eqs. (4) and (6). Eq. (5) is used to post process acoustic potential to obtain acoustic pressure and acoustic density from acoustic potential. The source is introduced at the source plane in terms of incident (right running) acoustic potential modal amplitudes. Reflected (left running) acoustic potential modal amplitudes are obtained as part of the solution. At the termination plane the acoustic field is represented by transmitted (right running) acoustic potential modal amplitudes and reflected (left running) acoustic potential modal amplitudes. The termination plane is assumed to be non-reflecting, and this is forced by requiring that reflected modal amplitudes vanish. Acoustic power is computed at the source plane and termination plane based on acoustic potential modal amplitudes by using the definition of Morfey [15], valid in the case of irrotational acoustic perturbations on irrotational mean flow. In addition, acoustic power is computed at any specified axial location using the Morfey definition, but by post-processing the acoustic potential. FEM modeling of acoustic propagation and radiation in non-uniform mean flow is presented in detail in Refs. [3,16]. Specific details of FEM applications to ducted flows terminated by reflection-free boundary conditions are presented in Refs. [11,12].

The outcome of the finite element approach to solving Eqs. (4) and (6) is in principle a linear system of equations

$$[A]\{x\} = \{f\}. \tag{22}$$

The vector $\{x\}$ is partitioned to include reflected modal amplitudes at the source plane $\{a^-\}$, acoustic potential values at interior nodes, and transmitted modal amplitudes at the termination $\{b^+\}$. The force vector $\{f\}$ is partitioned into the input modal amplitudes $\{a^+\}$ and a null vector for the remaining degrees of freedom:

$$\{f\} = \{a_1^+,\ a_2^+,\ \ldots a_{\mathrm{NPOS}}^+,\ 0,\ 0,\ \ldots\}^{\mathrm{T}}. \tag{23}$$

NPOS is the number of input modal amplitudes, generally equal to the number of cut-on modes plus a few additional modes. If these modal amplitudes are unknown, numerous random sets of modal magnitude and phase can be considered and duct propagation, for example attenuation, modeled in statistical terms. The FEM formulation for this can then be cast implicitly as

$$[A]\{x\} = [f], \tag{24}$$

where $[f]$ is a matrix of randomly constructed vectors with each column of the form of Eq. (23). In the investigation reported here, the matrix force $[f]$ may consist of as many as 100,000 randomly constructed forcing vectors. This form holds for each frequency and each circumferential mode. The forcing matrix has a potentially large number of columns suggesting many re-solutions of Eq. (24).

The set of linear equations in Eq. (22) never exist explicitly, as a frontal solver is used, and complete assembly of $[A]$ is not carried out. In the present study the frontal solver has been extended to accommodate multiple forcing vectors, making possible solutions to the set of equations implicitly described by Eq. (24). However, the number of columns in $[f]$ is limited, making it impractical to consider very large ensembles of randomly constructed input vectors. This limitation is overcome in the present analysis by noting that the number of input modal amplitudes, NPOS, is a relatively small number, less than 50 for the frequency range considered (NPOS is slightly larger than the number of propagating radial modes). This being the case, it is possible to generate NPOS independent solutions to Eq. (22) by constructing multiple forcing vectors in Eq. (24) with column j structured as

$$\{f_j\} = \left\{\delta_{1j},\ \delta_{2j},\ \ldots\ \delta_{ij}\ ,\ldots \delta_{\mathrm{NPOS},\,j},\ 0,\ 0,\ \ldots\right\}^{\mathrm{T}}, \tag{25}$$

where

$$\delta_{ij} = \begin{cases} 1, & i = j, \\ 0, & i \neq j. \end{cases}$$

Eq. (24) is solved with NPOS right-hand sides in $[f]$ described by Eq. (25). An influence coefficient matrix $[C]$ is then constructed with columns being the NPOS independent solutions generated in this way.

The solution for any randomly constructed modal input vector $\{a^+\}$ is then simply obtained by matrix multiplication:

$$\{x\} = [C]\{a^+\}. \tag{26}$$

Thus, after the efficient frontal solution of Eq. (25) with a relatively small number of right-hand sides, any number of solutions for the acoustic field, and metrics such as transmission loss, can be generated for randomly chosen input vectors via Eq. (26). This forms the basis for a statistical analysis of duct propagation, with statistical metrics such as mean transmission loss and the probability density for transmission loss based on a large sample space representing the acoustic source.

Each of the analysis methods has been coupled to an optimization algorithm. For the Cremer optimum, the optimization scheme searches for the maximum attenuation in a specified mode, typically the mode with the least attenuation. For the segmented duct code and the propagation code, the optimization scheme searches for the maximum attenuation of acoustic power. In the case of a circular duct where the outer wall has uniform lining, resistance and reactance are the two independent variables in the maximization algorithm. The downhill simplex method, due to Nelder and Mead [17], was used. It requires only function evaluations (the attenuation in our case) and not derivatives. The optimization process does not exclude the possible convergence to a local maximum, but experience has shown that the occurrence of such cases is rare.

3. Preliminary results

The Cremer optimum lining was determined for the least attenuated mode at the first blade passage frequency (BPF) in a uniform inlet of radius R, with a 16-blade rotor at supersonic tip speed. Inlet flow is at Mach number $M = -0.489$ and the non-dimensional frequency $\eta = 22.14$ is obtained using the relation $\eta = \pi Df/c$, where $D = 2R$ is the duct diameter, f the frequency in Hz and c the speed of sound of the mean flow. In the circumferential mode $m = 16$ two radial modes propagate. The treated section length is $l = 0.85$. Contours of equal attenuation are plotted in the impedance plane in Fig. 2.

The predicted optimum attenuation in the least attenuated mode is about 37 dB per distance equal to one duct radius, or equivalently, 31.45 dB considering the lining length $l = 0.85$. The optimum impedance, $Z = 3.57-1.28i$, was implemented in the segmented duct and propagation codes to compare the realized attenuation. Results obtained using the segmented duct procedure for the case when equal power is assumed in each of the two propagating modes are presented in Table 1. Seventeen choices of random phase produced by different seeds in a random number generator were used to complete the source model. A wide range of power attenuation values, dependent on phase, can be observed. Similar results were obtained under the equal modal amplitude assumption.

For $l = 0.85$, the Cremer optimum lining yields an attenuation of approximately 31.5 dB, higher than all but two of the occurrences in Table 1. To explain why this happens, three of the cases were examined further, one with a high attenuation, one with a medium attenuation and one with a low attenuation. Two propagating modes are incident at the source plane and two propagating modes are reflected and transmitted at the interface between the hard-wall source section and the lined section. In Table 2, the magnitudes and phases for both incident and scattered modes for the three cases are shown. Attenuation was calculated with both the segmented duct and propagation code (parentheses).

There is a distinct trend in the transmitted modal amplitudes that corresponds to the realized attenuation. As the attenuation decreases, the magnitudes of the transmitted modal amplitudes tend to equalize and the relative phase tends toward π radians. For the Cremer optimum impedance, the two modes tend to have similar radial pressure distribution. In the lined section acoustic power depends on modal magnitude and phase between modes. The combination of mode $n = 1$ and the out of phase mode $n = 2$ requires large amplitudes to carry the power initially incident from the source. Out of phase interaction tends to reduce acoustic pressure at the lining. The final effect is the reduction of attenuation below the attenuation levels for individual modes.

It is interesting to analyze here the contours of acoustic pressure for two fan inlet cases with identical modal magnitudes under the assumption of equal modal power in which only the phase distributions differ.

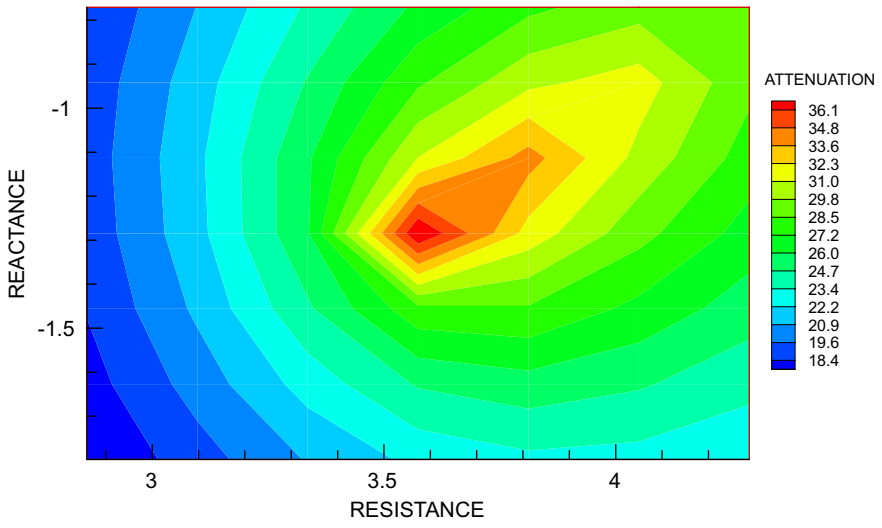

Fig. 2. Impedance plane contours of equal attenuation. $\eta_r = 22.14$, $m = 16$, $n = 1$ (least attenuated mode).

Table 1
Attenuation for seventeen cases of randomly chosen phases; two propagating modes

Case #	Attenuation (dB)	Case #	Attenuation (dB)
1	26.6	10	18.6
2	20.8	11	15.6
3	25.5	12	15.5
4	20.7	13	16.9
5	14.2	14	34.7
6	21.9	15	16.3
7	17.0	16	15.7
8	30.9	17	16.5
9	32.5		

$\eta_r = 22.14$, $m = 16$, $n = 1$, $l = 0.85R$. Segmented duct calculations with $Z = 3.57-1.28i$.

Table 2
Modal scattering and attenuation for two incident modes

Mode #	Input		Transmitted		Power attenuation
	Amplitude	Phase	Amplitude	Phase	
1	1	−1.35	1.49	−2.72	30.9
2	1.02	−2.92	0.84	−0.7	(31.1dB)
1	1	−1.32	12.89	2.05	20.7
2	1.02	−1.64	14.65	−1.15	(19.8dB)
1	1	−2.2	23.25	2.35	14.2
2	1.02	0.02	23.06	−0.82	(13.8dB)

$\eta_r = 22.14$, $m = 16$, $l = 0.85R$. Segmented duct and propagation code calculations with $Z = 3.57-1.28i$.

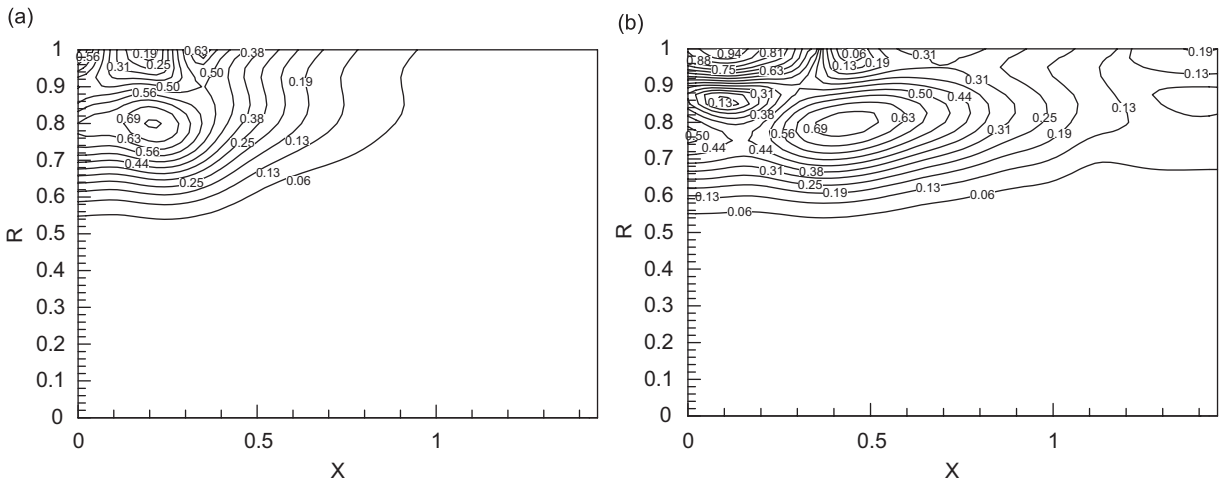

Fig. 3. Pressure level contours for two incident phase distributions, one producing high attenuation and the other low attenuation.

Cases 1 and 3 that were presented in Table 2 (cases 8 and 5 in Table 1) are considered. In Figs. 3a and b are shown contours of equal acoustic pressure magnitude, both normalized to the largest pressure on either plot.

In Fig. 3a is shown the acoustic field for the situation with high attenuation, 31.1 dB (propagation code). It is observed that the scattering process results in relatively high acoustic pressure at the lining, which extends

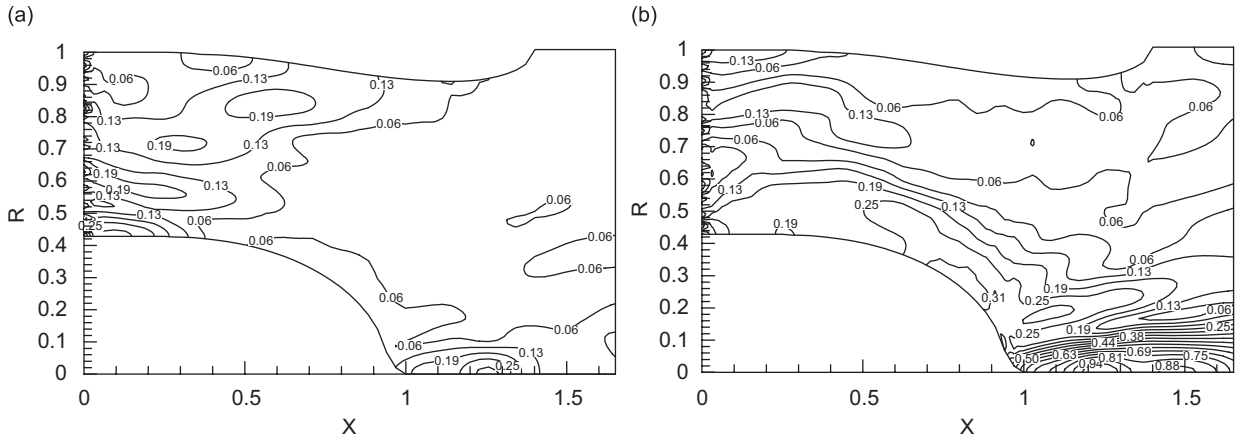

Fig. 4. Pressure level contours for two incident magnitude and phase distributions producing high and low attenuations, respectively.

from $x = 0.35$ to $x = 1.2$. From results in Fig. 3b, it can be seen that in the case of low attenuation, the scattering process results in relatively low acoustic pressure at the lining. In fact, higher acoustic pressures are channeled away from the outer wall. This last case has a much lower attenuation: 13.8 dB (propagation code). These two results suggest an explanation for differing lining performance, based on the acoustic field in the lined portion of the duct. In the high attenuation case initial phasing and scattering produce relatively high pressures at the initial portion of the lining on the outer wall. In the low attenuation case these effects combine to put the modes in the lined section out of phase and therefore destructively interfering at the initial portion of the lining on the outer wall.

The magnitudes of the incident modes along with their phase determine the attenuation. A case of a non-uniform duct with a contour and mean flow representative of a turbo-fan inlet reinforces this observation. The nacelle investigated in this study is based on the NASA Lewis ADP model scale inlet, with a scale factor of 5.91 [18,19]. For the duct geometry shown in Fig. 4, the non-dimensional frequency is $\eta = 30.25$, the circumferential mode is $m = 0$, and the flow has a speed of $M = -0.288$ (inlet flow). The inlet geometry has a hard wall center body while the outer wall has mainly resistive impedance, $Z = 2.86-0.01i$. The lining extends between $x = 0.5$ and $x = 1$. There are six propagating modes. In this case, modal magnitudes and phases are chosen randomly with the constraint that total normalized power is unity. A number of trials yielded a range of achieved attenuation. The normalized contour pressure levels for the case with the highest acoustic power attenuation obtained, 8.35 dB are shown in Fig. 4a, while the ones for the lowest attenuation, 0.21 dB are shown in Fig. 4b. It can be observed that in the low attenuation case the acoustic field is channeled toward the duct axis, while in the high attenuation case relatively higher acoustic pressure occurs along the treated wall.

4. Statistical source description for lining evaluation

It has been shown in the previous section that both the magnitude and phase of the incident modes affect acoustic attenuation in lined ducts. In this section, a more detailed analysis is carried out and distribution models for the total acoustic power at the exit of the duct and attenuation are obtained.

A relatively large number of unsystematic choices of magnitude and phase (arbitrarily selected by a random number generator provided with a "seed") are used to determine the range of attenuation for a given acoustic lining. Modal magnitude variation is accomplished indirectly by varying statistically the power in each propagating acoustic mode. Values of modal acoustic power and phase are assumed equally probable, so that uniform random numbers are generated. Non-uniform distributions can be used in case pre-existing information favors certain power or phase values.

4.1. Magnitude variation analysis

In most cases, insufficient or no reliable information is available about the noise source. A common way to partially deal with this lack of information is to make the assumption that propagating acoustic modal amplitudes have equal magnitude. Another hypothesis, used especially for broadband noise, is that the modes are distributed according to equal acoustic power per radial mode. Here it is assumed that the acoustic power in each incident radial mode varies randomly and independently of other modes while the phases at the source plane are held constant in all modes (not necessarily equal). Every modal power will be identically distributed in the interval (0, 1). It will be noticed in the following example that randomly powered incident modes will generate a total power at the exit of the duct the probability (or frequency of occurrence) of which seems to be normally distributed if relatively many modes contribute to it. This would be the case for a single low angular mode and/or a high frequency. In the immediately following investigation a single angular mode is assumed. A final case later assumes all propagating angular modes are present.

For the previously used inlet in Fig. 4, with Mach number $M = -0.416$ at a frequency $\eta = 50.75$, 100,000 random sets of incident radial modes forming the circumferential mode $m = 0$ are tested in the propagation code. In each set, the radial mode power is randomly distributed (uniform distribution) while the phases are equal. The lining impedance $Z = 3.0-3.0i$ is investigated. At this relatively high frequency and low mode number, 11 radial modes propagate at the source plane.

The acoustic power at the exit of the duct depends on the randomly powered set of incident modes. The resulting range of normalized exit power is divided in equal size bins (generally chosen as 0.3 times the standard deviation). The number of occurrences is calculated for each interval and a fraction is made with respect to the total number of trials, 100,000 in this case. This fractional number of occurrences plotted versus the exit power range produces what is here and throughout described as a probability density function for the total relative exit power that can be observed in Fig. 5a. In fact, a true probability density function with unit area under the curve would be the fractional occurrences per unit bin width. The results here are therefore scaled versions of the true density function. For comparison, a second case in which the circumferential mode is changed to $m = 28$ and having 6 propagating modes is presented in Fig. 5b. Also a third case with circumferential mode $m = 40$ with 3 propagating modes is shown in Fig. 5c.

It can be seen that a distribution that appears nearly Gaussian occurs even in the case with only 6 modes propagating. Yet, in the case with 3 modes propagating, the distribution of the power at the exit of the duct is skewed, with a longer tail to the right side. 100,000 sets of modes with randomly distributed power were used for the purpose of obtaining smooth distributions. This number has no influence on the general nature of the distribution of transmitted power, but a large number of samples increases the smoothness of the distribution curves. In Fig. 6 it is shown that the attenuation distribution for the same cases is skewed. More attenuation occurrences cluster in the low values, while higher values are less frequent. The mean attenuation is higher than the median. This is due to the logarithmic mapping of power into attenuation.

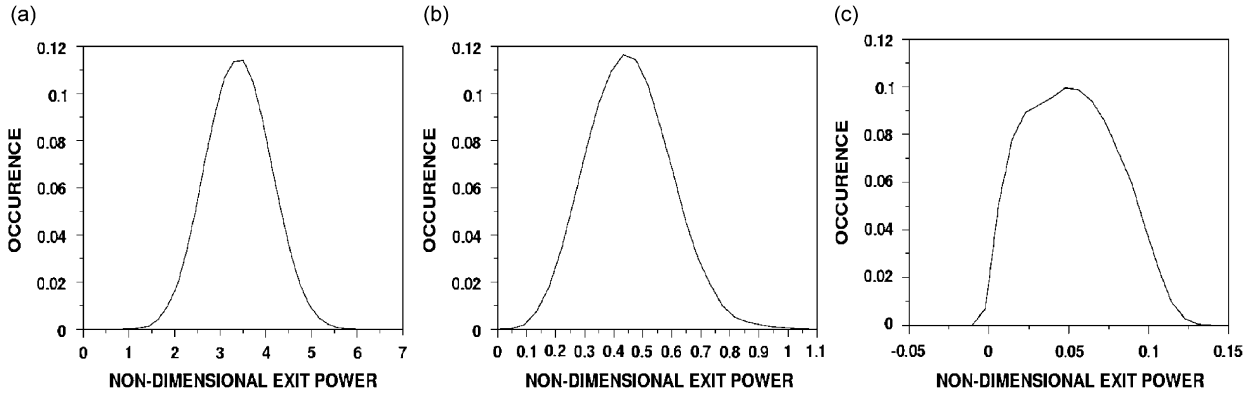

Fig. 5. Exit power distribution for three different angular modes. Non-uniform duct $\eta_r = 50.75$, $M = -0.416$, $Z = 3.0-3.0i$, equal incident modal phase, random power. (a) $m = 0$, (b) $m = 28$ and (c) $m = 40$.

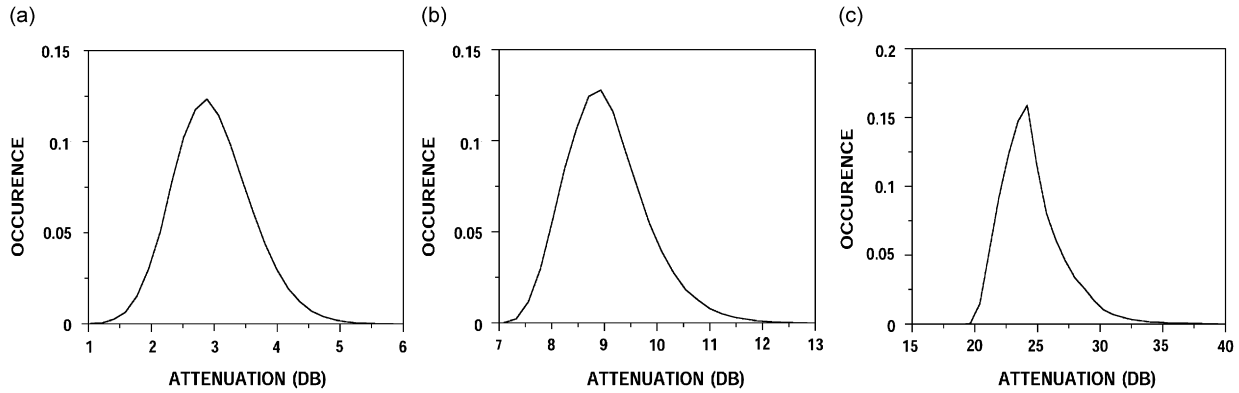

Fig. 6. Attenuation distribution for three different angular modes. Non-uniform duct. $\eta_r = 50.75$, $M = -0.416$, $Z = 3.0-3.0i$, equal incident modal phase, random power. (a) $m = 0$, (b) $m = 28$ and (c) $m = 40$.

Table 3
Comparison between propagation code (equal phase and random modal power) and test data for inlet at 1000 Hz, $M = -0.288$, $m = 0$

Model	Lining 1	Lining 2	Lining 3	Optimum
Equal modal power, 100,000 random modal phase cases	Outer wall impedance: (1.72 + 0.64i)	(2.34−0.58i)	(2.60−0.68i)	(1.74−0.35i)
Minimum (dB)	0.26	0.33	0.33	0.32
Mean (dB)	2.23	2. 38	2.33	2.44
Maximum (dB)	5.09	5.87	5.81	5.79
Standard deviation (dB)	0.67	0.728	0.71	0.75
Test (avg.) (dB)	2.18	2.58	2.80	

Comparison of predictions of the performance of acoustic treatment with experiment has historically not been very successful. Results of the present investigation suggest this is due to inadequate source modeling. The statistical prediction scheme based on random modal power is extended to explore broadband noise attenuation for which experimental data are available. For the ADP inlet geometry previously shown in Fig. 4, the attenuation for a case with many cut-on radial modes is considered by making use of the propagation code. At a fixed engine speed of 5750 rev/min, several frequencies in the noise spectrum, with no connection with blade and vane count judged not to be tonal, were studied. It is expected that broadband noise should be characterized by all circumferential and radial modes which propagate. In this initial comparison, the approach was to consider the single low order circumferential angular mode $m = 0$ to generate many propagating modes (a wide range of cut-off ratios), therefore, approximating the broadband conditions and producing attenuation comparable to the whole ensemble of propagating modes.

No test data for incident modal amplitudes were available, so a statistical analysis assuming equal phase with random incident modal power in angular mode $m = 0$ was conducted. Three acoustic linings identified as Linings 1, 2 and 3 were tested and results for frequencies of 1000 Hz ($\eta_r = 30.25$), 1250 Hz ($\eta_r = 37.82$), 1600 Hz ($\eta_r = 48.4$) and 2000 Hz ($\eta_r = 60.5$), are shown in Tables 3–6. The impedances of these three linings at the three frequencies are shown over the corresponding columns in the tables. The center body is not acoustically treated. The data values in the last column of these tables, labeled "Optimum", are for the impedance that maximizes the mean attenuation obtained over 100,000 random modal power cases. Original test results were reported in terms of sound pressure level (SPL) on a measurement arc in the radiated field for the hard wall configuration, as well as for the three considered linings. Data were available over the range of angles to the duct axis from 20° to 90°. Predictions are in terms of acoustic power attenuation. Sound pressure level data were converted to mean square pressure and integrated approximately over the hemisphere defined by the measurement arc with the assumption that on the arc acoustic intensity is proportional to mean square

Table 4
Comparison between propagation code (equal phase and random modal power) and test data for inlet at 1250 Hz, $M = -0.288$, $m = 0$

Model	Lining 1	Lining 2	Lining 3	Optimum
Equal modal power, 100,000 random modal phase cases	Outer wall impedance: (1.72 + 1.20i)	(2.34−0.18i)	(2.69−0.32i)	(2.38−0.14i)
Minimum (dB)	0.46	0.53	0.54	0.54
Mean (dB)	2.34	2.74	2.73	2.75
Maximum (dB)	5.25	6.07	6.00	6.08
Standard deviation (dB)	0.568	0.697	0.69	0.697
Test (avg.) (dB)	3.29	3.72	3.62	

Table 5
Comparison between propagation code (equal phase and random modal power) and test data for inlet at 1600 Hz, $M = -0.288$, $m = 0$

Model	Lining 1	Lining 2	Lining 3	Optimum
Equal modal power, 100,000 random modal phase cases	Outer wall impedance: (1.72 + 2.06i)	(2.34 + 0.27i)	(2.86−0.01i)	(2.24−0.25i)
Minimum (dB)	0.56	0.77	0.77	0.79
Mean (dB)	2.24	3.38	3.36	3.44
Maximum (dB)	4.38	7.86	7.73	8.21
Standard deviation (dB)	0.482	0.847	0.84	0.874
Test (avg.) (dB)	3.83	5.49	4.85	

Table 6
Comparison between propagation code (equal phase and random modal power) and test data for inlet at 2000 Hz, $M = -0.288$, $m = 0$

Model	Lining 1	Lining 2	Lining 3	Optimum
Equal modal power, 100,000 random modal phase cases	Outer wall impedance: (1.72 + 3.98i)	(2.34 + 0.73i)	(3.14 + 0.23i)	(2.38−0.12i)
Minimum (dB)	0.34	0.72	0.74	0.74
Mean (dB)	1.09	2.51	2.54	2.62
Maximum (dB)	2.11	6.10	6.14	6.47
Standard deviation (dB)	0.214	0.58	0.589	0.612
Test (avg.) (dB)	2.49	3.36	2.73	

acoustic pressure and directed normal to the calculation hemisphere. This equivalent experimental power attenuation was compared with calculated values.

From data in Tables 3–6, it can be seen that the numerical simulation showed that the performances of Linings 2 and 3 are about the same at the target frequencies tested and Lining 1 was the consistently least effective linear. It should be noted at this point that the minimum and maximum attenuation values shown in Tables 3–6, and all the subsequent ones, are obtained as a result of a statistical process. Another batch of random input modal amplitudes would produce different extreme values, nevertheless, in repeated numerical experiments there was little variation in the calculated extreme values. Test results have higher values of attenuation for both frequencies when compared with the mean values, except for the Lining 1 at 1000 Hz. However, the test data are plausible because, with one exception (Lining 1 at 2000 Hz), they all occur within

the range of results for the attenuation obtained in the random trials. It is interesting to note that the optimized lining did not provide a much better mean attenuation than Linings 2 and 3.

When the input modal power is varied, the highest values of attenuation are likely to be achieved when only the incident radial modes having the cut-off ratio closest to unity are powered. The probability of encountering cases in which only the low cut-off ratio modes are powered is very low considering all the possible power combinations in all the modes. Still, by considering a large number of random trials, such combinations occur, but the possibility of encountering an even higher value for attenuation must be emphasized. Similarly, the emergence of even lower values than the lows in the attenuation ranges seen in Tables 3–6 must not be excluded. On the other hand, 100,000 combinations of random incident modal power assures a stable estimated mean value so that a different set of 100,000 input random incident modal powers would produce an estimated mean attenuation very close to the previous one. The standard deviation estimate also varies little from one trial to another. Extreme values of attenuation (minimum and maximum) found in one trial of 100,000 random inputs may vary slightly from another trial. For a normal distribution around 95% of attenuation values occur within two standard deviations either side of the mean.

From these results, it is concluded that test results are, in most cases, within the statistical range predicted. With the modal input limited to $m = 0$, a good range of cut-off ratios is represented, and from the results of this exercise we suggest that this statistical approach based on a limited number of modes might be useful for design purposes. The possible disadvantage is that propagating $m = 0$ modes are skewed somewhat to high cut-off ratios as compared to a distribution of all propagating modes. Attenuation predictions may therefore be somewhat pessimistic. It is also noted that deviations from the mean for the probability density functions of Figs. 5 and 6 are large, and the inclusion of experimental results within the bounds shown is not conclusive proof that either predictions or experiment are good.

4.2. Phase variation analysis

Numerical experimentation presented previously showed that attenuation realized by an acoustically absorbing wall embedded in an otherwise hard wall duct is dependent on radial modal phasing when equal power or equal magnitude per mode is assumed. Because incident acoustic power in propagating modes in the hard wall section is dependent only on the modulus of the complex modal amplitudes, modal phasing can be set statistically with equal power assumed in each mode. Each modal phase takes up any value in the interval between 0 and 2π with equal probability of occurrence in this interval.

The cases presented previously in Fig. 5 are repeated, only this time the incident modal phases are varied randomly and the modal powers are considered equal. For the inlet geometry of Fig. 4, with a lining of impedance $Z = 3.0-3.0\mathrm{i}$, flow speed Mach number $M = -0.416$ and frequency $\eta = 50.75$, 100,000 sets of incident phases were chosen randomly while modal powers were set equal. Three angular modes were taken into account: $m = 0$, $m = 28$, $m = 40$, having 11, 6 and 3 propagating radial modes incident at the source, respectively. The total exit power, as shown in Fig. 7, is clearly not a normal distribution. There is a wider variation in exit power than when the incident modal power was varied randomly, if a comparison between Figs. 5 and 7 is made. In Fig. 8 is shown the corresponding attenuation distribution for the cases mentioned above.

Broadband noise attenuation test results previously presented in Tables 3–6 are once again compared with findings from a statistical investigation, this time assuming equal modal power with random incident modal phase, in circumferential mode $m = 0$. The numerical experiment was extended to 100,000 cases of random incident modal phases. Attenuation data in Tables 7–10 show qualitative similarity with attenuation data in Tables 3–6. Linings 2 and 3 produce comparable attenuations at the four target frequencies, while again Lining 1 performs worst. Attenuation ranges produced by random incident modal phases include averaged test results; still mean statistical values are lower than for the test data, especially for the higher frequency cases. Histogram presented in Figs. 9 and 10 provide a summary of attenuation probability distributions over many trials for the data in Tables 7 and 9. The histograms indicate that the attenuation results follow a skewed distribution with the right tail longer, a common feature for either randomly picked magnitude or phase. The simple right-skewed attenuation distribution model turns out to be less suitable with a decrease in the number of propagating modes. For Lining 1 at 1000 Hz, three cases with different numbers of cut-on modes were

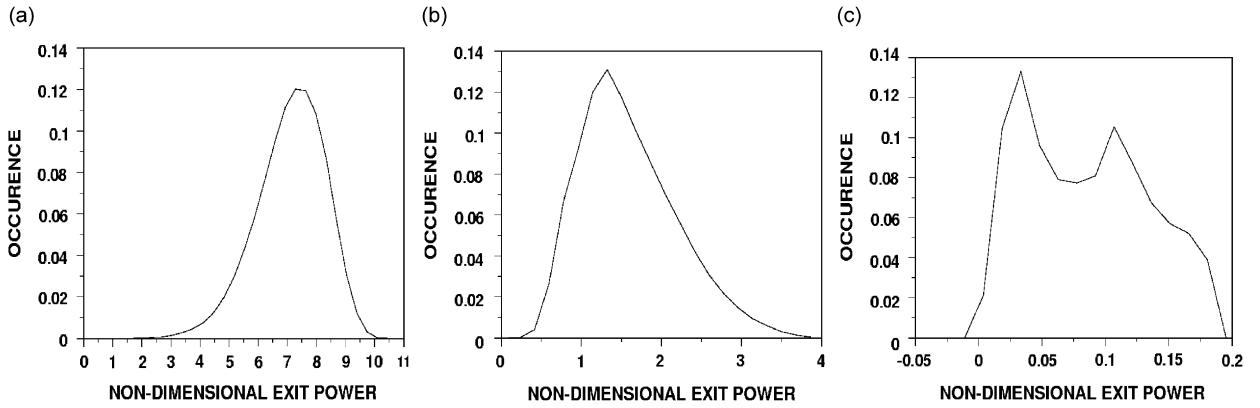

Fig. 7. Exit power distribution for three different angular modes. Non-uniform duct. $\eta_r = 50.75$, $M = -0.416$, $Z = 3.0-3.0i$, equal incident modal power, random phase. (a) $m = 0$, (b) $m = 28$ and (c) m = 40.

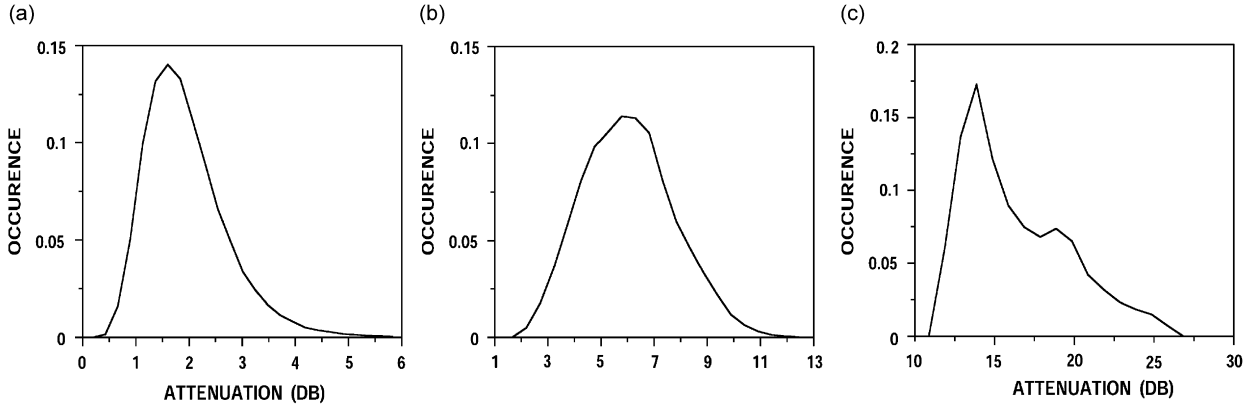

Fig. 8. Attenuation distribution for three different angular modes. Non-uniform duct. $\eta_r = 50.75$, $M = -0.416$, $Z = 3.0-3.0i$, equal incident modal power, random phase. (a) $m = 0$, (b) $m = 28$. and (c) $m = 40$.

Table 7
Comparison between propagation code (equal modal power, random phase) and test data for inlet at 1000 Hz, $M = -0.288$, $m = 0$

Model	Lining 1	Lining 2	Lining 3	Optimum
Equal modal power, 100,000 random modal phase cases	Outer wall impedance: (1.72 + 0.64i)	(2.34−0.58i)	(2.60−0.68i)	(2.46−0.72i)
Minimum (dB)	0.22	0.21	0.20	0.20
Mean (dB)	2.08	2.422	2.424	2.427
Maximum (dB)	8.90	14.66	14.06	14.64
Standard deviation (dB)	1.145	1.442	1.455	1.452
Test (avg.) (dB)	2.18	2.58	2.80	

considered. In Fig. 11a, an incident angular mode $m = 20$ was considered, with two equally powered cut-on radial modes then in Fig. 11b an angular mode $m = 18$ with three equally powered cut-on radial modes; and in Fig. 11c, an angular mode $m = 0$ with six equally powered cut-on radial modes. In each case, the relative phase of the angular modes was varied randomly with 100,000 random trials.

Table 8
Comparison between propagation code (equal modal power, random phase) and test data for inlet at 1250 Hz, $M = -0.288$, $m = 0$

Model	Lining 1	Lining 2	Lining 3	Optimum
Equal modal power, 100,000 random modal phase cases	Outer wall impedance: (1.72 + 1.20i)	(2.34−0.18i)	(2.69−0.32i)	(2.49−0.41i)
Minimum (dB)	0.47	0.46	0.44	0.45
Mean (dB)	2.13	2.557	2.559	2.57
Maximum (dB)	7.25	12.04	12.08	12.34
Standard deviation (dB)	0.887	1.198	1.215	1.215
Test (avg.) (dB)	3.29	3.72	3.62	

Table 9
Comparison between propagation code (equal modal power, random phase) and test data for inlet at 1600 Hz, $M = -0.288$, $m = 0$

Model	Lining 1	Lining 2	Lining 3	Optimum
Equal modal power, 100,000 random modal phase cases	Outer wall impedance: (1.72 + 2.06i)	(2.34 + 0.27i)	(2.86−0.01i)	(2.49−0.34i)
Minimum (dB)	0.36	0.40	0.38	0.38
Mean (dB)	1.66	2.34	2.35	2.38
Maximum (dB)	5.01	9.89	10.94	10.81
Standard deviation (dB)	0.61	0.977	1.009	1.017
Test (avg.) (dB)	3.83	5.49	4.85	

Table 10
Comparison between propagation code (equal modal power, random phase) and test data for inlet at 2000 Hz, $M = -0.288$, $m = 0$

Model	Lining 1	Lining 2	Lining 3	Optimum
Equal modal power, 100,000 random modal phase cases	Outer wall impedance: (1.72 + 3.98i)	(2.34 + 0.73i)	(3.14,0.23i)	(2.72−0.23i)
Minimum (dB)	0.16	0.36	0.35	0.35
Mean (dB)	0.93	2.10	2.17	2.22
Maximum (dB)	2.69	7.93	8.80	8.93
Standard deviation (dB)	0.325	0.818	0.875	0.893
Test (avg.) (dB)	2.49	3.36	2.73	

All three histograms shown in Fig. 11 show that the attenuation distribution is skewed toward the low range. If only two radial modes are propagating, there is only one relative phase that is varied randomly between 0 and 2π. The attenuation variation with relative phase for all 100,000 random phases is seen in Fig. 12a. This simple case shows that even though the relative phase variation produces high as well as low values of attenuation in a periodic manner, the low on the curve is more flat than the peak, favoring the occurrence of attenuation in the low range. The attenuation variation with phase is not perfectly sinusoidal, in which the lows are equally probable as the highs.

Attenuation variation with relative phase of the first two cut-on modes is shown in the graphs in Figs. 12b and c. For the 3 cut-on radial mode case, there are two more relative phases (between the first and the third and between the second and the third modes) that influence the attenuation. For the 6 cut-on radial mode case, there are fourteen more relative phases that also control attenuation. Because the radial modes are equally powered, all these relative phases influence the attenuation.

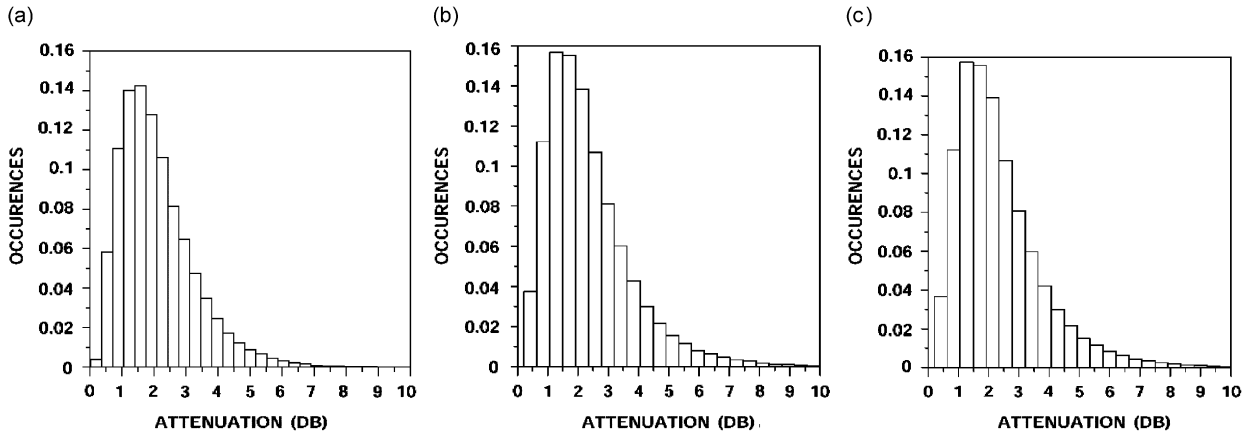

Fig. 9. Attenuation histograms for the Linings 1, 2 and 3 at 1000 Hz, $M = -0.288$, $m = 0$. (a) Lining 1, (b) lining 2 and (c) lining 3.

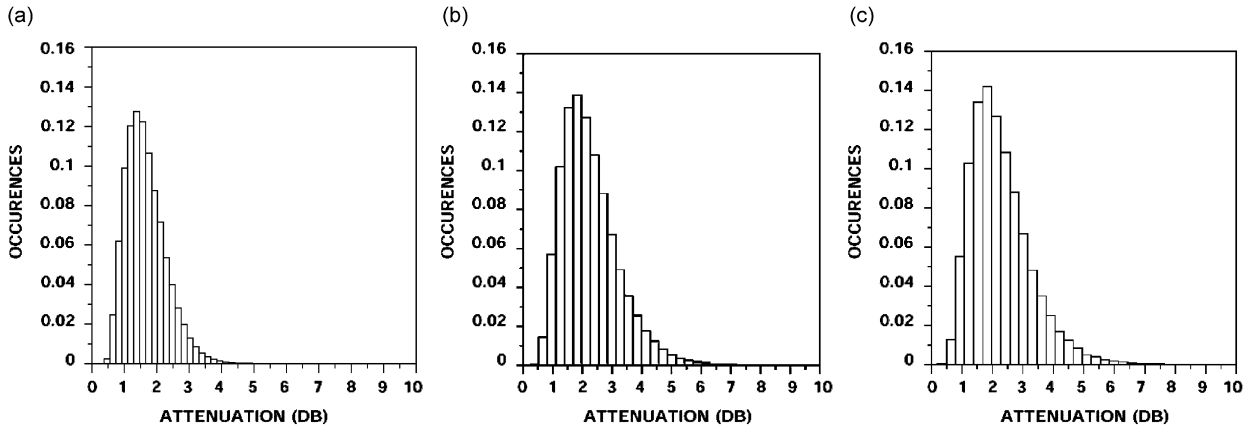

Fig. 10. Attenuation histograms for the Linings 1, 2 and 3 at 1600 Hz, $M = -0.288$, $m = 0$. (a) Lining 1, (b) lining 2 and (c) lining 3.

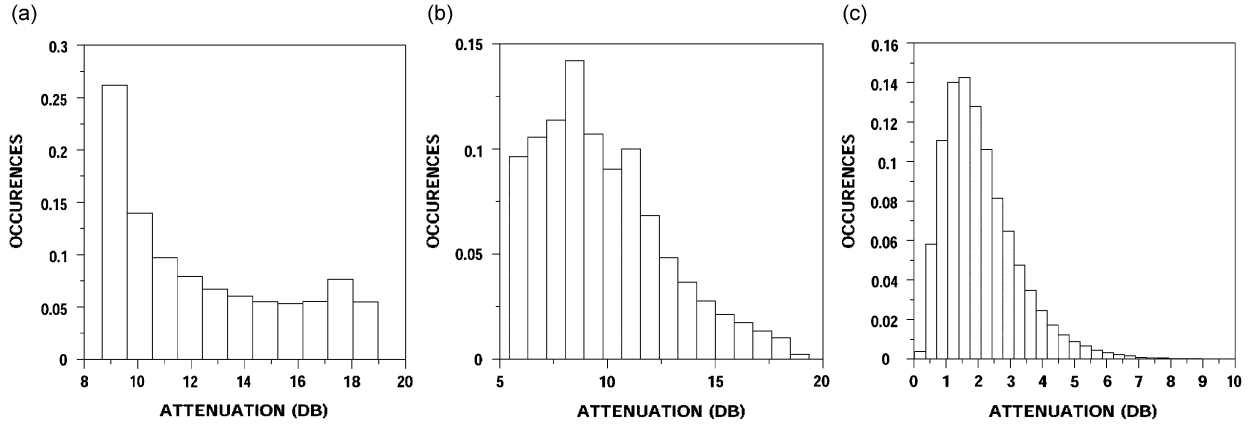

Fig. 11. Attenuation histograms for Lining 1, 1000 Hz, $M = -0.288$. (a) 2 cut-on radial modes, (b) 3 cut-on radial modes and (c) 6 cut-on radial modes.

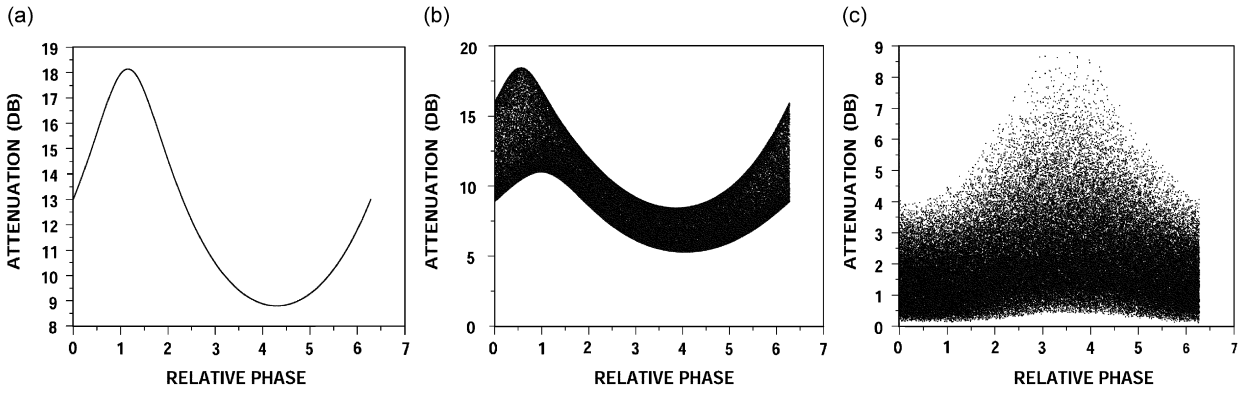

Fig. 12. Attenuation variation with relative phase for Lining 1, 1000 Hz, $M = -0.288$. (a) 2 cut-on radial modes, (b) 3 cut-on radial modes and (c) 6 cut-on radial modes.

For the attenuation to be substantial, attenuation should occur for most relative phases, but as the number of relative modes increases, the chance that all the relative phases would do so, is reduced. This is particularly evident in Fig. 12c, where there are only a few occurrences in the vicinity of 8.9 dB, which is the maximum attenuation achieved, while most attenuation values cluster in the low range.

In the hard wall section of the duct, the transmitted modes change relative phase while they propagate. The length of the hard wall section between the source plane and the non-uniform duct section will influence the phases of the modes incident on the non-uniform treated section, thus having a direct effect on the level of achieved attenuation. However, if the modal phase is randomly selected, statistically, the length of the hard-wall lead-in section will stop playing a role in the attenuation distribution. On the other hand, it is found that the location of the lining in the non-uniform section affects the attenuation distribution.

4.3. Magnitude and phase varying simultaneously

Whether incident modal powers were set randomly while modal phases were held fixed (Tables 3–6) or modal phases were set randomly while maintaining equal incident modal power (Tables 7–10) has only a minor effect on predictions and comparison with experiment, although attenuation in the experiments appear to be consistently higher than predicted mean attenuations.

If it is assumed that the experimental results are correct, and that measured (and post-processed) attenuations are consistently higher than the predictions, these results may indicate that the assumption of equal or random power in the radial modes is not sufficient in some cases, perhaps suggesting the use of a power distribution favoring modes that propagate at large angles from the axis (cut-off ratios close to unity), for example. In fact, Rice [9] has used a distribution biasing function based on the inverse powers of the cut-off ratio, but he proposed it for tonal noise, mentioning that the use of other functions is not excluded.

For Lining 1 at 1600 Hz, four modal power distributions, other than equal power were considered. The relative phases are randomly selected. The coefficients that adjust the power in each radial mode are given in Table 11. There are 10 cut-on radial modes and it can be observed that the first power distribution is one that emphasizes modes with low cut-off ratio. The second distribution accentuates radial modes with intermediate cut-off ratios and the third gives more power to modes with high cut-off ratio. A fourth distribution with totally random powers in the radial modes is also considered. In each case 100,000 randomly selected sets of incident amplitudes were considered.

To generate the first three power distributions, the following functions of the cut-off ratio were used:

1. $f_1(\xi) = 1/\xi^n$, with $n = 1$ (function suggested by Rice).
2. $f_2(\xi) = \exp[(-\xi - \xi_1)^2/2n]$, with $n = 1$ and $\xi_1 = 2.30$ corresponds to the cut-off ratio of mode 5.
3. $f_3(\xi) = (\xi/\xi_1)^n$ with $n = 0.3$ and ξ_1 the cut-off ratio of mode 1.

Table 11
4 modal power distributions, phases randomly selected

Mode #	Power coefficients for radial modes									
	1	2	3	4	5	6	7	8	9	10
Cut-off ratio	1×10^{6}	8.97	4.57	3.06	2.30	1.84	1.53	1.31	1.15	1.02
Distribution 1	0.001	0.114	0.224	0.334	0.445	0.556	0.667	0.778	0.889	1
Distribution 2	2×10^{-7}	6×10^{-4}	0.423	0.908	1	0.966	0.907	0.851	0.803	0.763
Distribution 3	1	0.243	0.199	0.176	0.162	0.151	0.143	0.137	0.131	0.127
Distribution 4	Random	Random	Random	Random	Random	Random	Random	Random	Random	Random

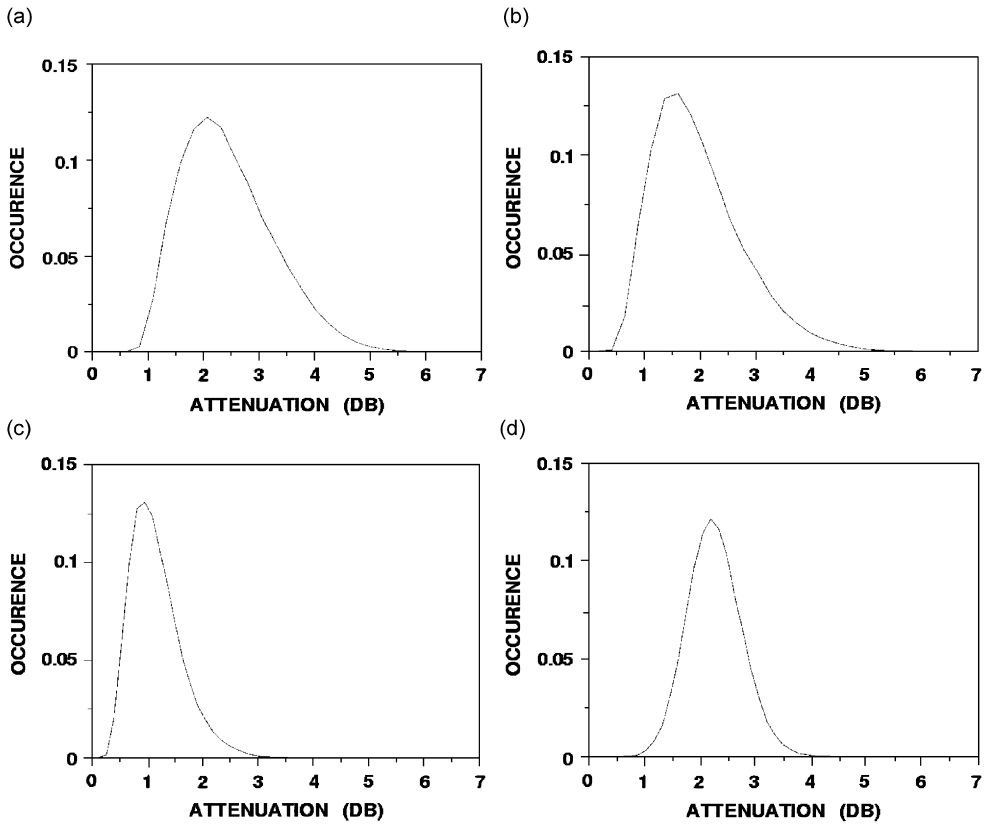

Fig. 13. Attenuation frequency plots of four different power distributions. (a) Distribution 1—favoring low cut-off ratio, (b) distribution 2—favoring intermediate cut-off ratios, (c) distribution 3—favoring high cut-off ratios and (d) distribution 4—random power and phase for all modes.

The relative attenuation frequency plot for the power distribution that emphasizes modes with low cut-off ratio is presented in Fig. 13a. The one providing more power to modes with intermediate cut-off ratios is shown in Fig. 13b, and the plot for modal power allocation that gives out more power to modes with a high cut-off ratio is shown in Fig. 13c. The plot for the case when both modal power and phase are selected randomly is presented in Fig. 13d.

Overall attenuation is reduced as high cut-off ratio modes are favored (distribution 3), while higher values of attenuation are obtained when low cut-off ratio modes are favored (distribution 1), as seen in Table 12. It can be observed that with the new models for power distribution in addition to randomly

Table 12
Attenuation ranges of 4 different power distributions

Distribution #	Minimum (dB)	Mean (dB)	Median (dB)	Maximum (dB)
1	0.78	2.44	2.33	6.33
2	0.42	1.96	1.82	5.95
3	0.24	1.16	1.09	3.58
4	0.09	1.66	1.58	5.13

Table 13
Comparison between propagation code and test data for inlet at 1000 Hz, $M = -0.288$, all angular modes considered

Model	Lining 1			Lining 2			Lining 3		
Equal modal phase, 100,000 random modal power cases	Outer wall impedance: (1.72 + 0.64i)			(2.34−0.58i)			(2.60−0.68i)		
	Model			Model			Model		
	1	2	3	1	2	3	1	2	3
Minimum (dB)	4.02	2.72	2.45	4.32	2.99	2.65	4.30	2.99	2.66
Mean (dB)	4.99	3.87	3.87	5.36	4.27	4.26	5.34	4.27	4.27
Maximum (dB)	6.19	5.42	5.56	6.74	6.22	6.23	6.69	6.24	6.23
Standard deviation (dB)	0.25	0.30	0.34	0.28	0.35	0.39	0.27	0.35	0.39
Test (avg.) (dB)	2.18			2.58			2.80		

distributed phase, the predicted ranges of achievable attenuations for Lining 1 at 1600 Hz, are higher in the case when strong low cut-off ratio modes are assumed (distribution 1 and to some extent distribution 2), but the means are still lower than the ones found in the experimental test.

4.4. Attenuation predictions based on all propagating modes

The method used up to this point to approximate broadband noise was to assess attenuation for angular mode $m = 0$ which produces radial modes with an extensive range of cut-off ratios. As has been seen in Tables 3–10, the result of this approach is a relatively wide attenuation range (a large standard deviation associated with the attenuation probability density function) that in general includes attenuation calculated from sound pressure level readings. The analysis is now taken a step further by calculating acoustic power attenuation for the whole group of incident angular modes that have cut-on radial modes at a given frequency. All incident acoustic powers in each angular mode are summed and similar summations are made for the reflected modal powers and the transmitted powers at the exit of the duct.

A first statistical investigation, named "Model 1", assuming equal phases with 100,000 random incident modal powers is carried out for Linings 1, 2 and 3 at the same 1000, 1250, 1600, and 2000 Hz frequencies. Then, in "Model 2", the same frequencies and linings are analyzed, only this time there are 100,000 cases of equal incident modal powers with random phases. In "Model 3" there are 100,000 cases of random incident modal phases and powers. The results are presented in Tables 13–16 for all three models.

An immediate observation is that the breadth of the probability density functions for attenuation are considerably reduced; note the small difference between minimum and maximum predicted attenuations in the tables. If test results are not within the calculated ranges of attenuation, they are close to them. It seems that the lower frequency attenuation results are over-predicted when compared with test data, while in the higher frequency range, the higher attenuations are closer to those found in the tests.

Table 14
Comparison between propagation code and test data for inlet at 1250 Hz, $M = -0.288$, all angular modes considered

Model	Lining 1			Lining 2			Lining 3		
Equal modal phase, 100,000 random modal power cases	Outer wall impedance: (1.72 + 1.20i)			(2.34−0.18i)			(2.69−0.32i)		
	Model			Model			Model		
	1	2	3	1	2	3	1	2	3
Minimum (dB)	3.85	2.33	2.47	4.41	2.68	2.83	4.42	2.70	2.85
Mean (dB)	4.58	3.53	3.56	5.32	4.12	4.15	5.32	4.14	4.17
Maximum (dB)	5.48	4.52	4.89	6.45	5.52	5.80	6.44	5.54	6.12
Standard deviation (dB)	0.19	0.21	0.24	0.24	0.28	0.31	0.24	0.28	0.31
Test (avg.) (dB)	3.29			3.72			3.62		

Table 15
Comparison between propagation code and test data for inlet at 1600 Hz, $M = -0.288$, all angular modes considered

Model	Lining 1			Lining 2			Lining 3		
Equal modal phase, 100,000 random modal power cases	Outer wall impedance: (1.72 + 2.06i)			(2.34 + 0.27i)			(2.86−0.01i)		
	Model			Model			Model		
	1	2	3	1	2	3	1	2	3
Minimum (dB)	3.41	2.05	2.03	4.53	2.57	2.54	4.55	2.63	3.00
Mean (dB)	3.93	3.01	3.02	5.26	3.95	3.96	5.28	4.00	4.00
Maximum (dB)	4.53	3.99	3.95	6.22	5.31	5.25	6.24	5.37	5.16
Standard deviation (dB)	0.13	0.13	0.16	0.19	0.21	0.23	0.19	0.22	0.24
Test (avg.) (dB)	3.83			5.49			4.85		

Table 16
Comparison between propagation code and test data for inlet at 2000 Hz, $M = -0.288$, all angular modes considered

Model	Lining 1			Lining 2			Lining 3		
Equal modal phase, 100,000 random modal power cases	Outer wall impedance: (1.72 + 3.98i)			(2.34 + 0.73i)			(3.14 + 0.23i)		
	Model			Model			Model		
	1	2	3	1	2	3	1	2	3
Minimum (dB)	1.75	1.66	1.58	3.02	2.72	2.58	3.16	2.79	2.61
Mean (dB)	2.00	1.92	1.92	3.46	3.21	3.21	3.60	3.30	3.30
Maximum (dB)	2.31	2.16	2.28	3.93	3.76	3.86	4.14	3.90	4.03
Standard deviation (dB)	0.06	0.06	0.08	0.11	0.12	0.15	0.11	0.13	0.19
Test (avg.) (dB)	2.49			3.36			2.73		

It is significant to observe here that mean attenuation results for Model 2 with random phase, equal modal power, and Model 3 characterized by random modal power and phase are, if not the same, within hundredths of each other for all four frequencies when all incident propagating modes are taken into consideration. This important observation supports a deduction by Dyer [20]. He proved that for narrow bands at high frequencies, when calculating time averaged random power in unlined ducts, the energy can be presumed

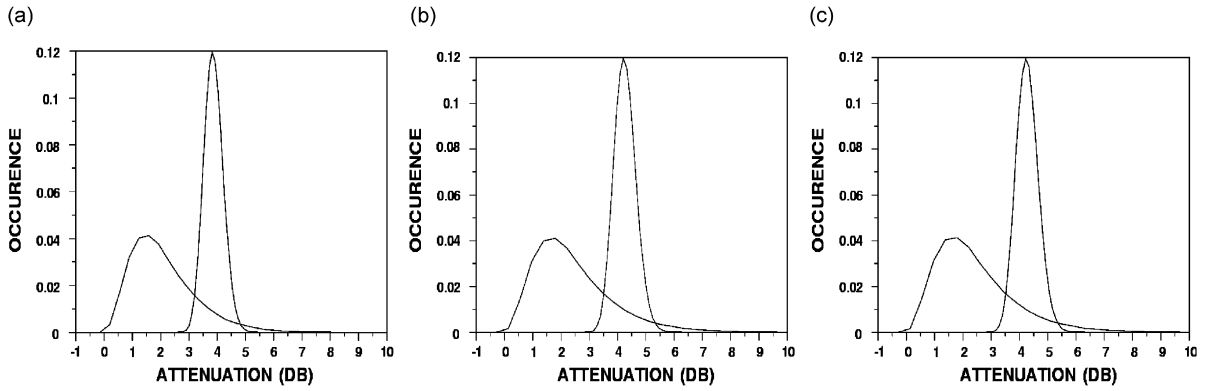

Fig. 14. Attenuation range comparison: mode $m = 0$ versus all propagating modes considered, for inlet at 1000 Hz, $M = -0.288$ (random incident modal power and phases): (a) lining 1, (b) lining 2 and (c) lining 3.

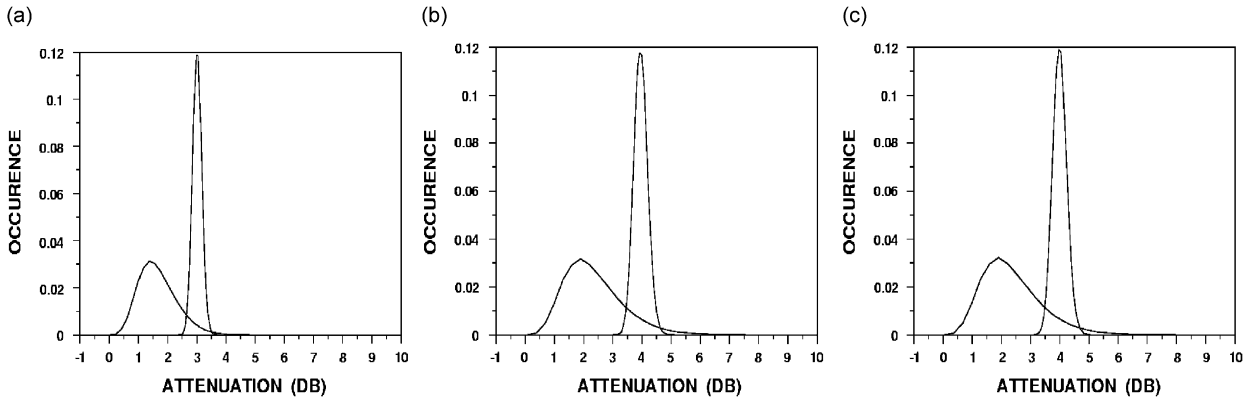

Fig. 15. Attenuation range comparison: mode $m = 0$ versus all propagating modes considered, for inlet at 1600 Hz, $M = -0.288$ (random incident modal power and phases): (a) lining 1, (b) lining 2 and (c) lining 3.

equally divided in all cut-on modes. Here it is shown that this conclusion can be extended to lined ducts as well. Model 1 in which equal phase with random incident modal power is assumed produced averaged results for attenuation that are higher than the ones for Models 2 and 3.

Comparison of results shown in Tables 7–10 with Model 1 results shown in Tables 13–16 reveal the shift and the compression in the attenuation range for all linings at all frequencies for the present situation, when all propagating modes are considered, as compared with the case when only propagating modes corresponding to the angular mode $m = 0$ were considered. A direct assessment of the above observation can be made with the help of Figs. 14 and 15 where attenuation of mode $m = 0$ is put side by side with the attenuation of all modes for the case of random incident modal power and phase at 1000 and 1600 Hz. The minimum and median attenuation are both shifted toward higher values, while the maximum attenuation decreases. The shift in attenuation toward higher values can be credited to the presence of radial modes with a low cut-off ratio that are easier to attenuate, brought in by taking into account higher order circumferential modes.

It should be noted here that comparison frequency plots in Figs. 14 and 15, and subsequently Fig. 16, represent fractional attenuation occurrence in bins with width 0.3 times the standard deviation for the $m = 0$ case. They represent scaled probability density functions, but can be compared on an equal basis.

A further important observation is made if all circumferential and radial propagating modes are considered and both modal power and modal phase are random. It was formerly found, in numerical experiments with many radial modes in the single circumferential mode $m = 0$, that an apparently normal distribution of transmitted acoustic power is achieved if the modal power is random but the phase is fixed. On the other hand, if modal power is held fixed and phase taken as random, the transmitted power was found not to be normally

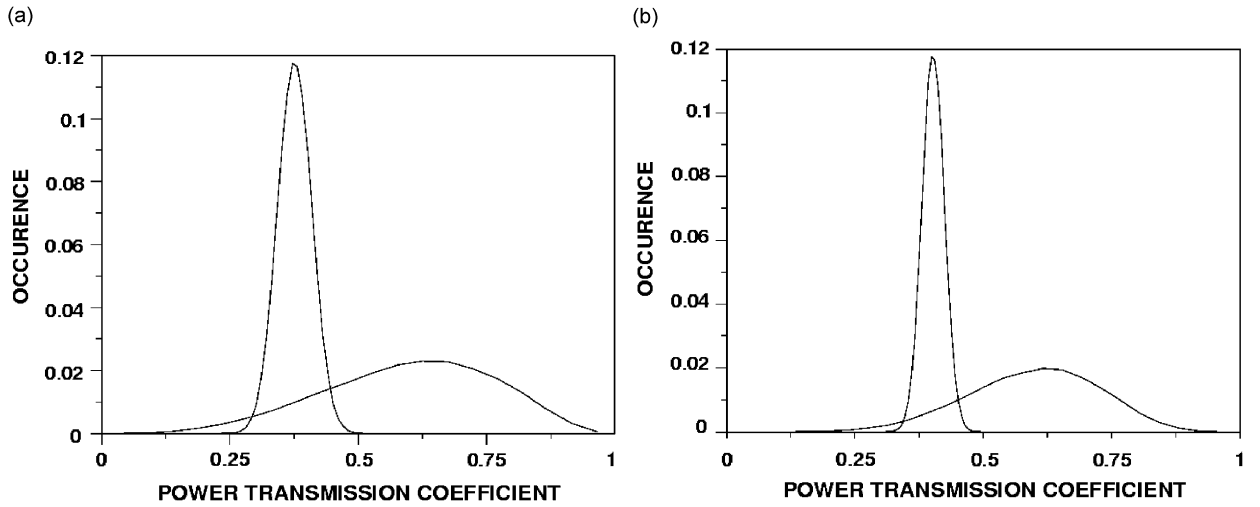

Fig. 16. Power transmission coefficient range comparison: mode $m = 0$ versus all propagating modes considered, for inlet at 1000 and 1600 Hz, $M = -0.288$, lining 2 (random incident modal power and phases). The narrower distribution corresponds to all propagating circumferential and radial modes. (a) 1000 Hz, (b) 1600 Hz.

Table 17
Comparison between propagation code (biased modal power emphasizing low cutoff-ratio modes) and test data for inlet at 1000 Hz, $M = -0.288$, all angular modes considered

Model	Lining 1	Lining 2	Lining 3
Rice biased modal power-100,000 random phase cases	Outer wall impedance: (1.72 + 0.64i)	(2.34−0.58i)	(2.60−0.68i)
Minimum (dB)	1.51	1.73	1.75
Mean (dB)	2.19	2.65	2.70
Maximum (dB)	3.17	3.94	4.05
Standard deviation (dB)	0.217	0.302	0.314
Test (avg.) (dB)	2.18	2.58	2.80

distributed. This observation was also made when both power and phase were random. The frequency of occurrence for random incident modal power and random phases for both the $m = 0$ case and the all propagating mode case is shown in Fig. 16. For a direct comparison, the plots in Fig. 16 are shown as a function of the power transmission coefficient, which is the total power at the exit divided by the total incident power. This is shown for the case of all propagating modes at 1000 and 1600 Hz.

The transmission coefficient appears to tend toward a Gaussian probability density function, even in these cases when incident modal phases are picked randomly. When only $m = 0$ was considered, the case of random power and random phase led to a non-Gaussian distribution for transmitted power.

A shift of the attenuation range could be achieved by using modal power biasing, as it was seen to be the case with mode $m = 0$. This process can be extended to the case when all propagating modes are considered in calculating acoustic attenuation. In this sense, at 1000 Hz, if modes with high cut-off ratio are predominant, lower attenuation should be achieved, while at 1600 Hz, at the source, the modes with low cut-off ratios should be getting more power than the modes with high cut-off ratios in order to get higher attenuation.

The modal power biasing function proposed by Rice, $f(\xi) = 1/\xi^n$, with $n = -0.67$ was tested for the 1000 Hz frequency, while the same function with $n = 1$ was tried for 1600 Hz. Results are presented in Tables 17 and 18. Test results are close to mean attenuation values. If attenuation derived from tests were to be matched by calculated values, for higher frequencies, incident modes with high cut-off ratio should be more heavily weighted, while at lower frequencies those with lower cut-off ratio should be more heavily weighted.

Table 18
Comparison between propagation code (biased modal power emphasizing low cutoff-ratio modes) and test data for inlet at 1600 Hz, $M = -0.288$, all angular modes considered

Model	Lining 1	Lining 2	Lining 3
Rice biased modal power-100,000 random phase cases	Outer wall impedance: (1.72 + 2.06i)	(2.34 + 0.27i)	(2.86−0.01i)
Minimum (dB)	2.79	3.41	3.43
Mean (dB)	3.89	5.04	5.03
Maximum (dB)	5.18	6.96	6.93
Standard deviation (dB)	0.153	0.246	0.246
Test (avg.) (dB)	3.83	5.49	4.85

Table 19
Estimated mean and standard deviation for 100, 1000, 10,000 and 100,000 combinations of random incident modal power and phases for $m = 0$, Lining 1

	1000 Hz		1250 Hz		1600 Hz		2000 Hz	
	Mean	Standard deviation	Mean	Standard deviation	Mean	Standard deviation	Mean	Standard deviation
100	3.17	1.39	2.21	0.92	1.63	0.59	1.69	0.71
1000	3.29	1.57	2.44	1.11	1.72	0.67	1.22	0.53
10,000	3.34	1.61	2.42	1.09	1.71	0.68	1.21	0.51
100,000	3.34	1.59	2.42	1.09	1.71	0.68	1.20	0.51

Table 20
Estimated mean and standard deviation for 100, 1000, 10,000 and 100,000 combinations of random incident modal power and phases, all angular modes considered, Lining 1

	1000 Hz		1250 Hz		1600 Hz		2000 Hz	
	Mean	Standard deviation	Mean	Standard deviation	Mean	Standard deviation	Mean	Standard deviation
100	3.88	0.404	3.52	0.345	2.99	0.245	1.90	0.099
1000	3.87	0.341	3.55	0.257	3.02	0.171	1.92	0.078
10,000	3.86	0.335	3.55	0.246	3.02	0.160	1.92	0.079
100,000	3.87	0.335	3.56	0.243	3.02	0.158	1.92	0.079

A matter of interest for the present investigation is the influence the size of the random modal input sample space has on the accuracy of the mean attenuation and standard deviation. In this sense, mode $m = 0$ and also the combination of all the propagating modes are studied, with 100, 1000, 10,000 and 100,000 random input modal power and phase combinations for Lining 1 at the 1000, 1250, 1600 and 2000 Hz frequencies.

In Table 19, it can be seen that for angular mode $m = 0$, 1000 random input modal combinations would provide good approximations for the average attenuation as well as for the distributional standard deviation, within approximately 1–2% of the corresponding reference values obtained for 100,000 random modal input combinations. The case of 100 random input combinations fails to obtain good estimates, this being especially evident for the 2000 Hz frequency. A total of 10,000 random modal power and phase sets produce attenuation with mean and standard deviations that are for all practical reasons, the same as those for the 100,000 random modal sets.

Table 20 shows that, similarly, when all propagating modes are considered, 1000 and 10,000 random modal power and phase combinations would yield attenuation mean values identical and standard deviation results very close to the ones resulting from a set of random modal power and phase combinations as big as 100,000.

5. Conclusions

The main goal of this study has been to explore the variation among analysis methods for the prediction of attenuation of lined turbofan inlet ducts. It has been demonstrated that details of the source model are critical in prediction of performance of acoustic treatment. Preliminary numerical experiments reveal that realized attenuation is strongly dependent on modal phasing and on scattering of incident modes at the interface between the hard wall source section and the acoustically treated section. More detailed analysis shows that realized attenuation is dependent on source details, and these may be uncertain. An acoustic treatment performance prediction method has emerged that provides for a statistical description of the source in terms of random modal power and random modal phase.

Specific findings include:

- For an acoustic lining imbedded in a hard wall duct, acoustic power transmission loss depends on the magnitude of the complex modal coefficients and strongly on the relative phase of the modes.
- A finite element duct propagation code has been developed for prediction of transmission characteristics with a statistically defined source model. Attenuation results are given in terms of probability distributions.
- Source descriptions examined include (a) random modal power and equal phase for all propagating radial modes for a single circumferential mode; (b) equal modal power and random phase for all propagating radial modes for a single circumferential mode; (c) random modal power and random phase for all propagating radial modes for a single circumferential mode; (d) modal power assigned with a biasing function and random phase for all propagating radial modes for a single circumferential mode; (e) random modal power and random phase for all propagating circumferential and radial modes for a single circumferential mode.
- For a single circumferential mode with a relatively large number of propagating radial modes, statistical distributions for transmitted power appear to be normally distributed (Gaussian) if modal power is random and phase is fixed or if modal power and phase are both random.
- For a single circumferential mode statistical distributions for transmitted power are not Gaussian if modal power is fixed or skewed with a biasing function and phase is random.
- For the case of all propagating circumferential and radial acoustic modes and with random modal power and phase, transmitted power appears to be normally distributed. This case produces statistical distributions with the least standard deviation, suggesting the sharpest estimate for realized attenuation.
- The several statistical models for realized attenuation have been compared to experimental data and the conclusion is drawn that in all cases a statistical source description produces better agreement with data than an unfounded assumption of modal input.

References

[1] L. Cremer, Theory of sound attenuation in rectangular ducts with absorbing walls and the resulting highest attenuation value, *Acoustics* 3 (2) (1953) 249–263.
[2] E.J. Rice, Inlet noise suppressor design method based on the distribution of acoustic power with mode cut-off ratio, *NASA CP*-2001, 1976.
[3] I. Danda Roy, W. Eversman, Far field calculations for turbofan noise, *AIAA Journal* 39 (12) (2001) 2255–2261.
[4] R.P. Dougherty, A parabolic approximation for flow effects on sound propagation in non-uniform, softwall ducts. *AIAA* 99-1822, 1999.
[5] R.P. Dougherty, Nacelle acoustic design by ray tracing in three dimensions. *AIAA* 96-1773, 1996.
[6] E.J. Rice, Attenuation of sound in soft-walled circular ducts, Aerodynamic Noise, *Proceedings of AFOSR-UTIAS Symposium*, Toronto, 20–21 May 1968, pp. 229–249.
[7] D.J. Snow, Influence of source characteristics on sound attenuation in a lined circular duct, *Journal of Sound and Vibration* 37 (1974) 459–465.
[8] S. Mariano, Effects of wall shear layers on the sound attenuation by broad band-width linings, *Acoustics* 29 (1973) 148–156.
[9] E.J. Rice, Multimodal far-field acoustic radiation pattern using mode cutoff ratio, *AIAA Journal* 9 (1978) 906–911.
[10] G. Zlavog, W. Eversman, Source effects on realized attenuation in lined ducts, Ninth AIAA/CEAS Aeroacoustics Conference, Hilton Head, NC, May 2003, *AIAA* 2003-3247, 2003.

[11] W. Eversman, A reverse flow theorem and acoustic reciprocity in compressible potential flow in ducts, *Journal of Sound and Vibration* 246 (1) (2001) 71–95.
[12] W. Eversman, Numerical experiments on acoustic reciprocity in compressible potential flows in ducts, *Journal of Sound and Vibration* 246 (1) (2002) 97–113.
[13] M.K. Myers, On the acoustic boundary condition in the presence of flow, *Journal of Sound and Vibration* 71 (1980) 429–434.
[14] W. Eversman, Theoretical models for duct acoustic propagation and radiation, in: H.H. Hubbard (Ed.), *NASA Technical Report RP*-1258 and *WRDC Technical Report TR* 90-3052, *Aeroacoustics of Flight Vehicles*, Noise Control, Vol. 2, August 1991, pp. 101–163.
[15] C.L. Morfey, Acoustic energy in non-uniform flows, *Journal of Sound and Vibration* 14 (1971) 159–170.
[16] I. Danda Roy, W. Eversman, Improved finite element modeling of the turbofan engine inlet radiation problem, *Journal of Vibration and Acoustics* 117 (10) (1995) 109–115.
[17] J.A. Nelder, R. Mead, *Computer Journal* 7 (1965) 308–311.
[18] L.J. Heidelberg, D.M. Elliott, A comparison of measured tone modes for two low noise propulsion fans, Sixth AIAA/CEAS Aeroacoustics Conference, Lahina, HI, May 2000, *AIAA* 2000-1989, 2000.
[19] G.W. Bielak, J.W. Premo, Advanced turbofan duct liner concepts, *NASA Technical Report CR*-1999-209002, 1999.
[20] I. Dyer, Measurement of noise sources in ducts, *Journal of Acoustical Society of America* 30 (1958) 833–841.